Application of a laser-based spectrometer for continuous insitu measurements of stable isotopes of soil CO₂ in calcareous and acidic soils

J. Joseph[1], C. Külls[2], M. Arend[3], M. Schaub[1], F. Hagedorn[1], A. Gessler[1] and M. Weiler[4]

[1] {Swiss Federal Institute for Forest, Snow and Landscape Research WSL, Zürcherstrasse 111, 8903 Birmensdorf, Switzerland}

[2] {Laboratory for Hydrology and International Water Management, University of Applied Sciences Lübeck, Germany}

[3] {Physiological Plant Ecology (PPE), Faculty of Integrative Biology, University of Basel, Switzerland}

[4] {Chair of Hydrology, Faculty of Environment and Natural resources, University of Freiburg, Germany}

Correspondence to: J. Joseph (jobin.joseph@wsl.ch)

Abstract

The short-term dynamics of carbon and water fluxes across the soil-plant-atmosphere continuum are still not fully understood. One important constraint is the lack of methodologies that enable simultaneous measurements of soil CO_2 concentration and respective isotopic composition at a high temporal resolution for longer periods of time. $\delta^{13}C$ of soil CO_2 can be used to derive information on the origin and physiological history of carbon and $\delta^{18}O$ in soil CO_2 aids to infer interaction between CO_2 and soil water. We established a real-time method for measuring soil CO_2 concentration, $\delta^{13}C$ and $\delta^{18}O$ values across a soil profile at higher temporal resolutions (0.05 – 0.1 hz) using an Off-Axis Integrated Cavity Output Spectrometer (OA-ICOS). We also developed a calibration method correcting for the sensitivity of the device against concentration-dependent shifts in $\delta^{13}C$ and $\delta^{18}O$ values under highly varying CO_2 concentration. The deviations of measured data were modelled, and a mathematical correction model was developed and applied for correcting the shift. By coupling an OA-ICOS with hydrophobic but gas permeable membranes placed at different depths in acidic and calcareous soils, we investigated the contribution of abiotic and biotic components to total soil CO_2 release. We found that in the calcareous Gleysol, CO_2 originating from carbonate dissolution contributed to the total soil CO_2 concentration at detectable degrees potentially due to CO_2 evasion from groundwater. ^{13}C-CO_2 of top soil at the calcareous soil site was found to be reflecting $\delta^{13}C$ values of atmospheric CO_2 and $\delta^{13}C$ of top soil CO_2 at the acidic soil site was representative of the biological respiratory processes. $\delta^{18}O$ values of CO_2 in both sites reflected the $\delta^{18}O$ of soil water across most of the depth profile, except for the 80 cm depth at the calcareous site where a relative enrichment in ^{18}O was observed.

Key words: $\delta^{13}C$, $\delta^{18}O$, OA-ICOS, hydrophobic/gas permeable membrane.

1   Introduction

Global fluxes of CO_2 and H_2O are two major driving forces controlling earth's climatic systems. To understand the prevailing climatic conditions and predict climate change, accurate monitoring and modeling of these fluxes are essential (Barthel et al., 2014; Harwood et al., 1999; Schär et al., 2004). Soil respiration, the CO_2 flux released from soil surface to the atmosphere as a result of microbial and root respiration (heterotrophic and autotrophic) is the second largest terrestrial carbon flux (Bond-Lamberty and Thomson, 2010). The long-term dynamics of CO_2 release on a seasonal scale are reasonably well understood (Satakhun et al., 2013), whereas less information on CO_2 dynamics and isotopic composition are available for short-term variations on a diurnal scale (Werner and Gessler, 2011). The lack of proper understanding of the diurnal fluctuations in soil CO_2 release might introduce uncertainty in estimating the soil carbon budget and the CO_2 fluxes to the atmosphere. The isotopic composition of soil CO_2 and its diel fluctuation can be a critical parameter for the partitioning of ecosystem gas exchange into its components (Bowling et al., 2003; Mortazavi et al., 2004) and for disentangling plant and ecosystem processes (Werner and Gessler 2011). By assessing $\delta1^3C$ of soil CO_2, it is possible to identify the source for CO_2 (Kuzyakov, 2006) and the coupling between photosynthesis and soil respiration when taking into account post-photosynthetic isotope fractionation (Werner et al., 2012; Wingate et al., 2010). $\delta^{13}C$ soil CO_2 reflects, however, not only microbial and root respiration but also abiotic sources from carbonate weathering (Schindlbacher et al., 2015).

Soil water imprints its $\delta^{18}O$ signature on soil CO_2 as a result of isotope exchange between H_2O and CO_2 (aqueous). The oxygen isotopic exchange between CO_2 and soil water is catalyzed by microbial carbonic anhydrase (Sperber et al., 2015; Wingate et al., 2009). Thus, soil CO_2 can give information on the isotopic composition of both soil water resources and carbon sources. The oxygen isotope composition of plant-derived CO_2 is both, a tracer of photosynthetic and respiratory CO_2 and gives additional quantitative information on the water cycle in terrestrial ecosystems (Francey and Tans, 1987). To better interpret the $\delta^{13}C$ and $\delta^{18}O$ signals of atmospheric CO_2, the isotopic composition and its variability of the different sources need to be better understood (Werner et al., 2012; Wingate et al., 2010).

The conventional method to estimate $\delta^{13}C$ and $\delta^{18}O$ of soil CO_2 efflux is by using two end-member mixing models of atmospheric CO_2 and CO_2 produced in the soil (Keeling, 1958). The conventional methods for sampling soil produced CO_2 are chamber based (Bertolini et al., 2006; Torn et al., 2003), 'mini-tower' (Kayler et al., 2010; Mortazavi et al., 2004), and soil gas well (Breecker and Sharp, 2008; Oerter and Amundson, 2016) based methods. In conventional methods, air sampling is done at specific time intervals, and $\delta^{13}C$ and $\delta^{18}O$ are analyzed using Isotope Ratio Mass Spectrometry (IRMS) (Ohlsson et al., 2005). Such offline methods have several disadvantages like high sampling costs, excessive time consumption for sampling and analysis, increased sampling error and low temporal resolution. Kammer et al. (2011), showed how error-prone the conventional methods could be while calculating $\delta^{13}C$ and $\delta^{18}O$ (up to several per mil when using chamber and mini tower-based methods) (Kammer et al., 2011). In chamber-based systems, non-steady-state conditions may arise within the chamber due to increased CO_2 concentrations which in turn hinders the diffusion of $^{12}CO_2$ more strongly than that of heavier $^{13}CO_2$ (Risk and Kellman, 2008). Moreover, it has been found that $\delta^{18}O$ of CO_2 inside a chamber is significantly influenced by the $\delta^{18}O$ of the surface soil water as an equilibrium isotopic exchange happens during the upward diffusive movement of soil CO_2 (Mortazavi et al., 2004). The advent of laser-based isotope spectroscopy has enabled cost-effective, simple, and high precision real-time measurements of $\delta^{13}C$ and $\delta^{18}O$ in CO_2 (Kammer et al., 2011; Kerstel

76 and Gianfrani, 2008). This technique opened up new possibilities for faster and reliable measurements of stable

77 isotopes insitu, based on the principle of light absorption, using laser beams of distinct wavelengths in the near and

78 mid-infrared range (Bowling et al., 2003). Recently, several high frequency online measurements of $\delta^{13}C$ and $\delta^{18}O$

79 of soil CO_2 and ^2H, ^{18}O of soil water vapor across soil depth profiles were reported by coupling either hydrophobic

80 but gas permeable membranes (installed at different depths in soil) or automated chamber systems with laser

81 spectrometers (Bowling et al., 2015; Jochheim et al., 2018; Stumpp et al., 2018). Such approaches enable detection

82 of vertical concentration profiles, temporal dynamics of soil CO_2 concentration and isotopic signature of soil CO_2

83 across different soil layers, thus aiding to identify and quantify various sources of CO_2 across the depth profile.

84 In 1988, O'Keefe and Decon introduced the Cavity Ring-Down Spectroscopy (CRDS) for measuring the isotopic

85 ratio of different gaseous species based on laser spectrometry (O'Keefe and Deacon, 1988). With the laser-based

86 spectrometry techniques, measuring sensitivities up to parts per trillion (ppt) concentrations are achieved (von

87 Basum et al., 2004; Peltola et al., 2012). In CRDS, the rate of change in the absorbed radiation of laser light that

88 is temporarily "trapped" within a highly reflective optical cavity is determined. This is achieved using resonant

89 coupling of a laser beam to the optical cavity and active locking of laser frequency to cavity length (Parameswaran

90 et al., 2009). Another well-established technique similar to CRDS is Off-Axis Integrated Cavity Output

91 Spectroscopy (OA-ICOS). It is based on directing lasers with narrowband and continuous-wave in an off-axis

92 configuration to the optical cavity (Baer et al., 2002).

93 Even though OA-ICOS can measure concentration and isotope signature of various gaseous species at high

94 temporal resolution, we found pronounced deviations in $\delta^{13}C$ and $\delta^{18}O$ measurements from the absolute values

95 when measured under changing CO_2 concentrations. So far to our knowledge, no study has been made available

96 detailing the calibration process of OA-ICOS CO_2 analyzers correcting for fluctuations of both $\delta^{13}C$ and $\delta^{18}O$

97 values under varying CO_2 concentrations. Most of the OA-ICOS CO_2 analyzers are built for working under stable

98 CO_2 concentrations, so that periodical calibration against in-house gas standards at a particular concentration is

99 sufficient. However, as there are pronounced gradients in CO_2 levels in soils (Maier and Schack-Kirchner, 2014),

100 CO_2 concentration depending shifts in measured isotopic values have to be addressed and corrected. Such

101 calibration is, however, also relevant for any other OA-ICOS application with varying levels of CO_2 (e.g., in

102 chamber measurements). Hence the first part of this work comprises the establishment of a calibration method for

103 OA-ICOS. The second part describes a method for online measurement of CO_2 concentrations and stable carbon

104 and oxygen isotope composition of CO_2 in different soil depths by coupling OA-ICOS with gas permeable

105 hydrophobic tubes (Membrane tubes, Accurel®). The use of these tubes for measuring soil CO_2 concentration (Gut

106 et al., 1998) and $\delta^{13}C$ of soil CO_2 (Parent et al., 2013) has already been established, but the coupling to an OA-

107 ICOS system has not been performed, yet.

108 We evaluated our measurement system by assessing and comparing the concentration, $\delta^{13}C$ and $\delta^{18}O$ of soil CO_2

109 for a calcareous and an acidic soil system. The primary foci of this study are to (1) introduce OA-ICOS in online

110 soil CO_2 concentration and isotopic measurements; (2) calibrate the OA-ICOS to render it usable for isotopic

111 analysis carried out under varying CO_2 concentrations; and (3) analyze the dynamics of $\delta^{13}C$ and $\delta^{18}O$ of soil CO_2

112 at different soil depths in different soil types at a higher temporal resolution.

113

2   Materials and Methods

2.1   Instrumentation

The concentration, $\delta^{13}C$ and $\delta^{18}O$ values of CO_2 were measured with an OA-ICOS, as described in detail by Baer et al. (2002) and Jost et al. (2006). In this study, we used an OA-ICOS, (LGR-CCIA 36-d) manufactured by Los Gatos Research Ltd, San-Francisco, USA. LGR-CCIA 36-d measures CO_2 concentration, and $\delta^{13}C$ and $\delta^{18}O$ values at a frequency up to 1 Hz. The operational CO_2 concentration range was 400 to 25,000 ppm. Operating temperature range was +10 - +35°C, and sample temperature range (Gas temperature) was between -20°C and 50°C. Recommended inlet pressure was < 0.0689 MPa. The multiport inlet unit, an optional design that comes along with LGR-CCIA 36-d, had a manifold of 8 digitally controlled inlet ports and one outlet port. It rendered the user with an option of measuring eight different CO_2 samples at the desired time interval. Three standard gases with distinct $\delta^{13}C$ and $\delta^{18}O$ values were used for calibration in this study (See Supplementary Table.1). The standard gases used in this study were analyzed for absolute concentration and respective $\delta^{13}C$ and $\delta^{18}O$ values. δ-values are expressed based on Vienna Pee Dee Belemnite (VPDB)-CO_2 scale, and were determined by high precision IRMS analysis.

2.2   Calibration setup and protocol

We developed a two-step calibration procedure to; a) correct for concentration-dependent errors in isotopic data measurements, and b) correct for deviations in measured δ-values from absolute values due to offset (other than concentration-dependent error) introduced by the laser spectrometer. Also, we used Allan variance curves for determining the time interval to average the data (Nelson et al., 2008) to achieve the highest precision that can be offered by LGR-CCIA 36-d (Allan et al., 1997).

The first part of our calibration methodology was developed to correct for the concentration-dependent error observed in preliminary studies for $\delta^{13}C$ and $\delta^{18}O$ values measured using OA-ICOS. Such a calibration protocol was used in addition to the routine three-point calibration performed with in-house CO_2 gas standards of known $\delta^{13}C$ and $\delta^{18}O$ values. We developed a CO_2 dilution set up (See Figure. 1), with which each of the three CO_2 standard gases was diluted with synthetic CO_2 free air (synth-air) to different CO_2 concentrations. By applying a dilution series, we identified the deviation of the measured (OA-ICOS) from the absolute (IRMS) $\delta^{13}C$ and $\delta^{18}O$ values depending on CO_2 concentration (See Figure.4). The $\delta^{13}C$ and $\delta^{18}O$ values of our inhouse calibration gas standards were measured via cryo-extraction and Dual Inlet IRMS. $\delta^{13}C$, and $\delta^{18}O$ of the standard gases (See Supplementary Table.1) across a wide range of CO_2 concentrations are measured using OA-ICOS. The deviation of the measured $\delta^{13}C$, and $\delta^{18}O$ from absolute values with respect to changing CO_2 concentrations was mathematically modeled and later used for data correction (See Figure.5). A standard three-point calibration was then applied correcting for concentration-dependent errors (See Figure.7). The standards used covered a wide range of $\delta^{13}C$ and $\delta^{18}O$, including the values observed in the field of application.

Standard gases were released to a mass flow controller (ANALYT-MTC, series 358, MFC1) after passing through a pressure controller valve (See Figure. 1) with safety bypass (TESCOM, D43376-AR-00-X1-S; V5). A Swagelok

filter, ((Stainless Steel All-Welded In-Line Filter (Swagelok, SS-4FWS-05; F1)) was installed at the inlet of the flow controller (ANALYT-MTC, series 358; MFC1). Synth-air was released and passed to another flow controller (ANALYT-MTC, series 358; MFC2) through a Swagelok filter (F2 in Figure. 1). CO_2 and synth-air leaving the flow controllers (MFC1 and MFC2 respectively) were then mixed and drawn through a 6.35 mm outer diameter (OD) Teflon tube (P8), which was kept in a gas thermostat unit (See Figure.1). The thermostat unit contained, a) a thermostat-controlled water bath (Kottermann, 3082) and b) an Isotherm flask containing liquid nitrogen. The water bath was used to raise the temperature above room temperature and also to bring the temperature down to +5°C, by placing ice packs in the water bath. To reach low temperatures (-20°C), we immersed the tubes in the isotherm flask filled with liquid N_2. Leaving the thermostat unit, the gas was directed to the multiport inlet unit of the OA-ICOS. By using the thermostat unit, we introduced a shift in the reference gas temperature and the aim was to test the temperature sensitivity of the OA-ICOS in measuring $\delta^{13}C$ and $\delta^{18}O$ values. The third CO_2 standard gas (which is used for validation) was produced by mixing the other two gas standards in equal molar proportions in a 10L volume plastic bag with inner aluminum foil coating and welded seams (CO_2 mix: Linde PLASTIGAS®) under 0.03 MPa pressure by diluting to the required concentration using synth-air. The mixture was then temperature adjusted and delivered to the multiport inlet unit (MIU) by using a 6.35 mm (OD) Teflon tube (P10). From the multiport inlet unit, calibration gases were delivered into the OA-ICOS for measurement using a 6.35 mm (OD) Teflon tube (P9) at a pressure < 0.0689 MPa, with a flow rate of 500 mL/min. The gas leaving the OA-ICOS through the exhaust was fed back to the 6.35 mm (OD) Teflon tube (P8) by using a Swagelok pipe Tee (Stainless Steel Pipe Fitting, Male Tee, 6.35 mm (OD). Male NPT), intersecting P8 line before entering the thermostat unit. Thus, the gas fed was looped in the system until steady values were reported by the OA-ICOS based on CO_2 [ppm], $\delta^{13}C$ and $\delta^{18}O$ measurements. CO_2 gas standards were measured at 27 different CO_2 concentration levels ranging between 400 and 25,000 ppm. Every hour before sampling, synth-air gas was flushed through the system to remove CO_2 to avoid memory effects. The calibration gases were measured in a sequence one after the other four times. During each round of measurement, every calibration gas was diluted to different concentrations of CO_2 (400 - 25,000 ppm) and the respective isotopic signature and concentration were determined. For each measurement of $\delta^{13}C$ and $\delta^{18}O$ at a given concentration, the first 50 readings were omitted to avoid possible memory effects of the laser spectrometer and the subsequent readings for the next 256 seconds were taken and averaged to get maximum precision for $\delta^{13}C$ and $\delta^{18}O$ measurements. When switching between different calibration gases at the multiport inlet unit, synth-air was purged through the systems for 30 seconds to avoid cross-contamination.

2.3 Experimental Sites

In situ experiments were conducted to measure $\delta^{13}C$, $\delta^{18}O$ and concentrations of soil CO_2 in two different soil types (calcareous and acidic soil). The measurements in a calcareous soil were conducted during June 2014 in cropland cultivated with wheat (*Triticum aestivum*) in Neuried, a small village in the Upper Rhine Valley in Germany situated at 48°26'55.5"N, 7°47'20.7"E, 150 m a.s.l. The soil type described as calcareous fluvic Gleysol IUSS (2014) developed on gravel deposits in the upper Rhine valley. Soil depth was medium to deep, with high contents of coarse material (> 2 mm) up to 30 - 50%. Mean soil organic carbon (SOC) content was 1.2 - 2% and,

186 SOC stock was ranging between 50 and 90 t/ha. The average pH was found to be 8.6. The study site receives an
187 annual rainfall of 810 mm and has a mean annual temperature of 12.1°C.

188 In situ measurements in an acidic soil were conducted by the end of July 2014 in the model ecosystem facility
189 (MODOEK) of the Swiss Federal Research Institute WSL, Birmensdorf, Switzerland (47°21'48" N, 8°27'23" E,
190 545 m a.s.l.). The MODOEK facility comprises 16 model ecosystems, belowground split into two lysimeters with
191 an area of 3 m^2 and a depth of 150 cm. The lysimeters used for the present study were filled with acidic (haplic
192 Alisol) forest soil IUSS (2014) and planted with young beech trees (Arend et al., 2016). The soil pH was 4.0 and
193 a total SOC content of 0.8% (Kuster et al., 2013).

194 **2.4   Experimental Setup**

195 The OA-ICOS was connected to gas permeable, hydrophobic membrane tubes (Accurel® tubings, 8 mm OD) of
196 2 m length, placed horizontally in the soil at different depths. Tubes were laid in six different depths (4, 8, 12, 17,
197 35, and 80 cm) for calcareous soil and three (10, 30, and 60 cm) for acidic soil.

198 Technical details of the measurement setup are shown in Figure 2. Both ends of the membrane tubes were extended
199 vertically upwards reaching the soil top by connecting them to gas impermeable Synflex® tubings (8 mm OD)
200 using Swagelok tube fitting union (Swagelok: SS-8M0-6, 8 mm Tube OD). One end of the tubing system was
201 connected to a solenoid switching valve (Bibus: MX-758.8E3C3KK) and by using a stainless-steel reducing union
202 (Swagelok: SS-8M0-6-6M), to the outlet of the LGR CCIA 36-d by using 6.35 mm (OD) Teflon tubing. The other
203 end was connected via the multiport inlet unit to the gas inlet of the LGR CCIA 36-d.

204 This way, a loop was created in which the soil CO_2 drawn into the OA-ICOS was circulated back through the tubes
205 and in and out of the OA-ICOS and measured until a steady state was reached. We experienced no drop in cavity
206 pressure while maintaining a closed loop (See Supplementary Figure S2). Each depth was selected and
207 continuously measured for 6 minutes at specified time intervals by switching to defined depths at the multiport
208 inlet unit and also at the solenoid valve.

209

210 **3   Results and Discussion**

211 **3.1   Instrument calibration and correction**

212 The highest level of precision obtained for $\delta^{13}C$ and $\delta^{18}O$ measurements at the maximum measuring frequency
213 (1Hz) were determined by using Allan deviation curves (see Figure 3).   Maximum precision of 0.022‰ for $\delta^{13}C$
214 was obtained when the data were averaged over 256 seconds, and for $\delta^{18}O$, 0.077‰ for the same averaging interval
215 as for $\delta^{13}C$.

216 To correct for CO_2 concentration-dependent errors in raw $\delta^{13}C$ and $\delta^{18}O$ data, we analysed data obtained from the
217 OA-ICOS to determine the sensitivity of $\delta^{13}C$ and $\delta^{18}O$ measurements against changing concentrations of CO_2. We
218 observed a specific pattern of deviance in the measured isotopic data from the absolute values (both for $\delta^{13}C$ and

219 $\delta^{18}O$) across CO_2 concentration ranging from 25,000 to 400 ppm (See Figure.4). Uncalibrated $\delta^{13}C$ and $\delta^{18}O$
220 measurements showed a standard deviation of 6.44 ‰ and 6.80 ‰ respectively, when measured under changing
221 CO_2 concentrations.

222 The dependency of $\delta^{13}C$ and $\delta^{18}O$ values on the CO_2 concentration was compensated by using a nonlinear model.
223 The deviations (Diff-δ) of the measured delta values ($\delta_{(OA\text{-}ICOS)}$) from the absolute value of the standard gas (δ
224 $_{(IRMS)}$) at different concentrations of CO_2 were calculated (Diff-δ = $\delta_{(OA\text{-}ICOS)}$ - $\delta_{(IRMS)}$). Several mathematical
225 models were then fitted on Diff-δ as a function of changing CO_2 concentration (See figure.5). The mathematical
226 model with the best fit for Diff-δ data was selected using Akaike information criterion corrected (AICc) (Glatting
227 et al., 2007; Hurvich and Tsai, 1989; Yamaoka et al., 1978). The non-linear model fits applied for Diff-$\delta^{13}C$, and
228 Diff-$\delta^{18}O$ measurements are given in Tables 1 & 2, respectively. For Diff-$\delta^{13}C$, a three-parameter exponential
229 model fitted best with r^2 = 0.99 (see Table 3 for the values of the parameters, see supplementary Figure S3 (a) for
230 model residuals), and a three-parameter power function model (see Table 2) with r^2 = 0.99 showed the best fit for
231 Diff-$\delta^{18}O$ (see Table 3 for the values of the parameters, see supplementary Figure S3 (b) for model residuals). The
232 best fit was then introduced into the measured isotopic data ($\delta^{13}C$ and $\delta^{18}O$) and corrected for concentration-
233 dependent errors (See figure. 6). After correction, the standard deviation of $\delta^{13}C$ was reduced to 0.08 ‰ and of
234 $\delta^{18}O$ to 0.09 ‰ for all measurements across the whole CO_2 concentration range.

235

236 After correcting the measured $\delta^{13}C$ and $\delta^{18}O$ values for the CO_2 concentration-dependent deviations, a three-point
237 calibration (Sturm et al., 2012) was made by generating linear regressions with the concentration corrected $\delta^{13}C$
238 and $\delta^{18}O$ values against absolute $\delta^{13}C$ and $\delta^{18}O$ values (See Figure.7, see supplementary Figure S4 for linear
239 regression residuals). Using the linear regression lines, we were able to measure the validation gas standard with
240 standard deviations of 0.0826 ‰ for $\delta^{13}C$ and 0.0941 ‰ for $\delta^{18}O$.

241 For the LGR CCIA 36-d, we found that routine calibration (Correction for concentration-dependent error plus
242 three-point calibration) was necessary for obtaining the required accuracy, in particular under fluctuating CO_2
243 concentrations. The LGR CCIA-36d offers an option for calibration against a single standard, a feature which was
244 already in place in a predecessor model (CCIA DLT-100) (Guillon et al., 2012). This internal calibration is
245 sufficient, when LGR CCIA-36d is operated only under stable CO_2 concentrations. To correct for the concentration
246 dependency, we introduced mathematical model fits, which corrected for the deviation pattern found for both $\delta^{13}C$
247 and $\delta^{18}O$. We assume that these deviations are instrument specific and the fitting parameters need to be adjusted
248 for every single device. Experiments conducted to investigate the influence of external temperature fluctuations
249 on OA-ICOS measurements did not show any significant changes in the temperature inside the optical cavity of
250 OA-ICOS (See Supplementary Figure S1). The previous version of the Los Gatos CCIA was strongly influenced
251 by temperature fluctuations during sampling (Guillon et al., 2012). The lack of temperature dependency as
252 observed here with the most recent model can be mostly due to the heavy insulation provided with the system,
253 which was not found in the older models.

254 Guillon et al. (2012) found a linear correlation between CO_2 concentration and respective stable isotope signatures
255 with a previous version of the Los Gatos CCIA CO_2 stable isotope analyser. In our experiments with the OA-ICOS,
256 best fitting correlation between CO_2 concentration and $\delta^{13}C$ and $\delta^{18}O$ measurements were exponential and power

functions, respectively. We assume that measurement accuracy is influenced by the number of CO_2 molecules present inside the laser cavity of the particular laser spectrometer as we observed large standard deviation in isotopic measurements at lower CO_2 concentrations. This behavior of an OA-ICOS can be expected as it functions by sweeping the laser along an absorption spectrum, measuring the energy transmitted after passing through the sample. Therefore, energy transmitted is proportional to the gas concentration in the cavity. The laser absorbance is then determined by normalizing against a reference signal, finally calculating the concentration of the sample measured by integrating the whole spectrum of absorbance (O'Keefe et al., 1999).

3.2 Variation in soil CO_2 concentration, carbon and oxygen isotope values

Figures 9 and 10 show the CO_2 concentration, $\delta^{13}C$ and $\delta^{18}O$ measurements of soil CO_2 in the calcareous as well as in the acidic soil across the soil profile with sub-daily resolution and as averages for the day, respectively. We observed an increase in the CO_2 concentration across the soil depth profile for both, the calcareous and the acidic soil. Moreover, there were rather contrasting $\delta^{13}C$ values across the profile for the two soil types. In the calcareous soil, CO_2 was relatively enriched in ^{13}C in the surface soil (4 cm) as compared to the 8 cm depth. Below 8 cm down to 80 cm depth, we found an increase in $\delta^{13}C$ values. At 80 cm depth, the $\delta^{13}C$ in soil CO_2 ranged between -7.15 and -3.35 ‰ (See Figure. 9) with a daily average of -6.19 ± 1.45 ‰ (See Figure. 10) and hence clearly above atmospheric values ($\approx$ -8.0 ‰). For $\delta^{18}O$ values of calcareous soil, the depth profile showed no specific pattern except for the $\delta^{18}O$ values at 80 cm depth was found to be less negative than the values of the other depths. The $\delta^{18}O$ value in the top 4 cm was found to be slightly more enriched that the 8 cm depth and between 8 cm – 35 cm, $\delta^{18}O$ values showed little variation relative to each other. For the sub-daily measurements, we observed a sharp decline in $\delta^{18}O$ values at around 02:00, which is also observed but less pronounced for $\delta^{13}C$ signal. We assume that, the reason for such aberrant values is rather a technical issue than a biological process. It could be due to the fact that the internal pump in the OA-ICOS was not taking adequate amount of gas into the optical cavity, thereby creating a negative pressure inside the cavity resulting in the observed aberrant values. The patterns observed for the $\delta^{13}C$ values of CO_2 in the calcareous soil with ^{13}C enrichment in deeper soil layers can be explained by a substantial contribution of CO_2 from abiotic origin to total soil CO_2 release as a result of carbonate weathering and subsequent out-gassing from soil water (Schindlbacher et al., 2015). According to Cerling (1984), the distinct oxygen and carbon isotopic composition of soil carbonate depends primarily on the isotopic signature of meteoric water and to the proportion of C_4 biomass present at the time of carbonate formation (Cerling, 1984), but also on numerous other factors that determine the ^{13}C value of soil CO_2. CO_2 released as a result from carbonates in calcareous soil site have a distinct $\delta^{13}C$ value of -9.3 (mean value across soil profile 0 - 80 cm depth) (Figure 8(c)), while CO_2 released during biological respiratory processes has $\delta^{13}C$ values around -24‰ as observed in the acidic soil (Figure 10 (e)). The $\delta^{13}C$ values of soil CO_2 observed in the deepest soil layer in the calcareous soil site most likely indicates the presence of carbonate sources of pedogenic and geologic origin. Even though the contribution of CO_2 from abiotic sources to soil CO_2 is often considered to be low, several studies have reported significant proportions ranging between (10 - 60%) emanating from abiotic sources (Emmerich, 2003; Plestenjak et al., 2012; Ramnarine et al., 2012; Serrano-Ortiz et al., 2010; Stevenson and Verburg, 2006; Tamir et al., 2011). Bowen and Beerling, (2004) showed that isotope effects associated with soil organic matter decomposition can cause a strong gradient in δ values of soil organic matter (SOM) with depth, but are not always reflected in the $\delta^{13}C$ values of soil

295   CO_2. We have measured soil samples for bulk soil $\delta^{13}C$, carbonate $\delta^{13}C$ & $\delta^{18}O$ values and also determined the

296   percentage of total carbon in the soil across a depth profile of (0-80 cm) (See Figure 8). We observed an increase

297   in $\delta^{13}C$ values for bulk soil in deeper soil layers (See Figure 8 (a,c)). Moreover, also the carbonate $\delta^{13}C$ values got

298   more positive in the 60-80 cm layer. Since total organic carbon content decreases with depth it can be assumed

299   that CO_2 derived from carbonate weathering having less negative $\delta^{13}C$ more strongly contributed to the soil CO_2

300   (especially since we see an increase in soil CO_2 concentration with depth). This is accordance with the laser-based

301   measurements which showed a strong increase in $\delta^{13}C$ of soil CO_2 in the deepest soil layer leading us to the

302   hypothesis that this signal is indicating a strong contribution of carbonate derived CO_2. Water content, soil CO_2

303   concentration and presence of organic acids or any other source of H^+ are the major factors influencing carbonate

304   weathering, and variations in soil CO_2 partial pressure, moisture, temperature, and pH can cause degassing of CO_2

305   which contributes to the soil CO_2 efflux (Schindlbacher et al., 2015; Zamanian et al., 2016). $CaCO_3$ solubility in

306   pure H_2O at 25°C is 0.013 gL^{-1}, but in weak acids like carbonic acid, the solubility is increased up to five fold

307   (Zamanian et al., 2016). The production of carbonic acid due to CO_2 dissolution will convert carbonate to

308   bicarbonates resulting in exchange of carbon atoms between carbonates and dissolved CO_2. We assume that at our

309   study site, the topsoil is de-carbonated due to intensive agriculture for a longer period and thus soil CO_2 there

310   originates primarily from autotrophic and heterotrophic respiratory activity. In contrast to the deeper soil layers,

311   where the carbonate content is high, CO_2 from carbonate weathering is assumed to be a dominating source of soil

312   CO_2. Also, outgassing of CO_2 from the large groundwater body underneath the calcareous Gleysol might contribute

313   to the inorganic CO_2 sources in the deeper soil as we found ground water table to be 1-2m below the soil surface.

314   Relative ^{13}C enrichment of the CO_2 in the topsoil (4 cm) compared to 8 cm depth is probably due to the invasive

315   diffusion of atmospheric CO_2 which has a $\delta^{13}C$ value close to -8‰ (e.g., (Levin et al., 1995)). The $\delta^{18}O$ patterns

316   for CO_2 between 4 and 35 cm might reflect the $\delta^{18}O$ of soil water with stronger evaporative enrichment at the top

317   and ^{18}O depletion towards deeper soil layers. In comparison, the strong ^{18}O enrichment of soil CO_2 towards 80 cm

318   in the calcareous Gleysol very likely reflects the ^{18}O values of groundwater lending further support for the high

319   contribution of CO_2 originating from the outgassing of groundwater. We, however, need then to assume that that

320   the oxygen in the CO_2 is not in full equilibrium with the precipitation influenced soil water. As mainly microbial

321   carbonic anhydrase mediates the fast equilibrium between CO_2 and water in the soil and the microbial activity is

322   low in deeper soil layers (Schmidt et al., 2011), we speculate that in deep layers with a significant contribution of

323   ground-water derived CO_2 to the CO_2 pool, a lack of full equilibrium with soil water might be the reason for the

324   observed $\delta^{18}O$ values.

325

326   Soil CO_2 concentration in the acidic soil showed a positive relationship with soil depth as CO_2 concentration

327   increased along with increasing soil depth (Figs. 9 & 10). CO_2 concentrations were distinctly higher than in the

328   calcareous soil, very likely due to the finer texture than in the gravel-rich calcareous soil. $\delta^{13}C$ values amounted to

329   approx. – 26 ‰ in 30 and 60 cm depth indicating the biotic origin from (autotrophic and heterotrophic) soil

330   respiration (Schönwitz et al., 1986). In the topsoil, $\delta^{13}C$ values did not strongly increase, pointing towards a less

331   pronounced inward diffusion of CO_2 in the acidic soil site, most likely due to more extensive outward diffusion of

332   soil CO_2 as indicated by the still very high CO_2 concentration at 10 cm creating a sharp gradient between soil and

333   atmosphere. Moreover, the acidic soil was rather dense and contained no stones, strongly suggesting that gas

334 diffusivity was rather small. $\delta^{18}O$ depths patterns of soil CO_2 in the acidic soil were most likely reflecting $\delta^{18}O$
335 values of soil water as CO_2 became increasingly ^{18}O depleted from top to bottom. $\delta^{18}O$ of deeper soil layers CO_2
336 (30 - 60 cm) was close to the values expected when full oxygen exchange between soil water and CO_2 occurred
337 (Kato et al., 2004). Assuming an ^{18}O fractionation of 41‰ between CO_2 and water (Brenninkmeijer et al., 1983)
338 this would result in an expected value for CO_2 of $\approx$ -10 $\pm$ 2‰ vs. VPDB-CO_2. Corresponding results had been
339 shown for $\delta^{18}O$ of soil CO_2 using similar hydrophobic gas permeable membrane tubes used when measuring $\delta^{18}O$
340 of soil CO_2 and soil water *in situ* (Gangi et al., 2015).

341 **4 Conclusions**

342 During our preliminary tests with the OA-ICOS, we found that the equipment was highly sensitive to changes in
343 CO_2 concentrations. We found a non-linear response of the $\delta^{13}C$ and $\delta^{18}O$ values against changes in CO_2
344 concentration. Given the fact that laser-based CO_2 isotope analyzers are deployed on site in combination with
345 different gas sampling methods like automated chambers systems (Bowling et al., 2015), and hydrophobic gas
346 permeable membranes (Jochheim et al., 2018) for tracing various ecosystem processes, it is important to address
347 this issue. Therefore, we developed a calibration strategy for correcting errors introduced in $\delta^{13}C$ and $\delta^{18}O$
348 measurements due to the sensitivity of the device against changing CO_2 concentrations. We found that the OA-
349 ICOS measures stable isotopes of CO_2 gas samples with a precision comparable to conventional IRMS. The
350 method described in this work for measuring CO_2 concentration, $\delta^{13}C$ and $\delta^{18}O$ values in soil air profiles using an
351 OA-ICOS and hydrophobic gas permeable tubes are promising and can be applied for soil CO_2 flux studies. As
352 this set up is capable of measuring continuously for longer time periods at higher temporal resolution (0.05 $-$ 0.1
353 Hz), it offers greater potential to investigate the isotopic identity of CO_2 and the interrelation between soil CO_2 and
354 soil water. By using our measurement setup, we could identify abiotic as well as biotic contributions to the soil
355 CO_2 in the calcareous soil. We infer that that degassing of CO_2 from carbonates due to weathering and evasion of
356 CO_2 from groundwater may leave the soil CO_2 with a specific and distinct $\delta^{13}C$ signature especially when the biotic
357 activity is rather low.

358

359

366

367

368

11

References

Allan, D. W., Ashby, N. and Hodge, C. C.: The Science of Timekeeping, Hewlett-Packard, 88 [online] Available from: http://www.allanstime.com/Publications/DWA/Science_Timekeeping/TheScienceOfTimekee ping.pdf (Accessed 16 March 2018), 1997.

Arend, M., Gessler, A. and Schaub, M.: The influence of the soil on spring and autumn phenology in European beech, edited by C. Li, Tree Physiol., 36(1), 78–85, doi:10.1093/treephys/tpv087, 2016.

Baer, D. S., Paul, J. B., Gupta, M. and O'Keefe, A.: Sensitive absorption measurements in the near-infrared region using off-axis integrated-cavity-output spectroscopy, Appl. Phys. B Lasers Opt., 75(2–3), 261–265, doi:10.1007/s00340-002-0971-z, 2002.

Barthel, M., Sturm, P., Hammerle, A., Buchmann, N., Gentsch, L., Siegwolf, R. and Knohl, A.: Soil $H_2^{18}O$ labelling reveals the effect of drought on $C^{18}OO$ fluxes to the atmosphere, J. Exp. Bot., 65(20), 5783–5793, doi:10.1093/jxb/eru312, 2014.

von Basum, G., Halmer, D., Hering, P., Mürtz, M., Schiller, S., Müller, F., Popp, A. and Kühnemann, F.: Parts per trillion sensitivity for ethane in air with an optical parametric oscillator cavity leak-out spectrometer, Opt. Lett., 29(8), 797, doi:10.1364/OL.29.000797, 2004.

Bertolini, T., Inglima, I., Rubino, M., Marzaioli, F., Lubritto, C., Subke, J.-A., Peressotti, A. and Cotrufo, M. F.: Sampling soil-derived CO_2 for analysis of isotopic composition: a comparison of different techniques, Isotopes Environ. Health Stud., 42(1), 57–65, doi:10.1080/10256010500503312, 2006.

Bond-Lamberty, B. and Thomson, A.: Temperature-associated increases in the global soil respiration record, Nature, 464(7288), 579–582, doi:10.1038/nature08930, 2010.

Bowen, G. J. and Beerling, D. J.: An integrated model for soil organic carbon and CO_2: Implications for paleosol carbonate p CO_2 paleobarometry, Global Biogeochem. Cycles, 18(1), n/a-n/a, doi:10.1029/2003GB002117, 2004.

Bowling, D. R., Sargent, S. D., Tanner, B. D. and Ehleringer, J. R.: Tunable diode laser absorption spectroscopy for stable isotope studies of ecosystem–atmosphere CO2 exchange, Agric. For. Meteorol., 118(1–2), 1–19, doi:10.1016/S0168-1923(03)00074-1, 2003.

399   Bowling, D. R., Egan, J. E., Hall, S. J. and Risk, D. A.: Environmental forcing does not induce
400   diel or synoptic variation in the carbon isotope content of forest soil respiration, Biogeosciences,
401   12, 5143–5160, doi:10.5194/bg-12-5143-2015, 2015.

402   Breecker, D. and Sharp, Z. D.: A field and laboratory method for monitoring the concentration
403   and isotopic composition of soil CO_2, Rapid Commun. Mass Spectrom., 22(4), 449–454,
404   doi:10.1002/rcm.3382, 2008.

405   Brenninkmeijer, C. A. M., Kraft, P. and Mook, W. G.: Oxygen isotope fractionation between
406   CO2 and H2O, Chem. Geol., 41, 181–190, doi:10.1016/S0009-2541(83)80015-1, 1983.

407   Cerling, T. E.: The stable isotopic composition of modern soil carbonate and its relationship to
408   climate, Earth Planet. Sci. Lett., 71(2), 229–240, doi:10.1016/0012-821X(84)90089-X, 1984.

409   Emmerich, W. E.: Carbon dioxide fluxes in a semiarid environment with high carbonate soils,
410   Agric.   For.   Meteorol.,   116,   91–102   [online]   Available   from:
411   http://citeseerx.ist.psu.edu/viewdoc/download?doi=10.1.1.457.6452&rep=rep1&type=pdf
412   (Accessed 16 March 2018), 2003.

413   Fao: World reference base for soil resources 2014 International soil classification system for
414   naming soils and creating legends for soil maps Update 2015 WORLD SOIL RESOURCES
415   REPORTS, [online] Available from: http://www.fao.org (Accessed 21 January 2019), n.d.

416   Francey, R. J. and Tans, P. P.: Latitudinal variation in oxygen-18 of atmospheric CO2, Nature,
417   327(6122), 495–497, doi:10.1038/327495a0, 1987.

418   Gangi, L., Rothfuss, Y., Ogée, J., Wingate, L., Vereecken, H. and Brüggemann, N.: A New
419   Method for In Situ Measurements of Oxygen Isotopologues of Soil Water and Carbon Dioxide
420   with High Time Resolution, Vadose Zo. J., 14(8), 0, doi:10.2136/vzj2014.11.0169, 2015.

421   Glatting, G., Kletting, P., Reske, S. N., Hohl, K. and Ring, C.: Choosing the optimal fit function:
422   Comparison of the Akaike information criterion and the F-test, Med. Phys., 34(11), 4285–4292,
423   doi:10.1118/1.2794176, 2007.

424   Guillon, S., Pili, E. and Agrinier, P.: Using a laser-based CO2 carbon isotope analyser to
425   investigate gas transfer in geological media, Appl. Phys. B, 107(2), 449–457,
426   doi:10.1007/s00340-012-4942-8, 2012.

427   Gut, A., Blatter, A., Fahrni, M., Lehmann, B. E., Neftel, A. and Staffelbach, T.: A new
428   membrane tube technique (METT) for continuous gas measurements in soils, Plant Soil, 198(1),

429   79–88, doi:10.1023/A:1004277519234, 1998.

430   Harwood, K. G., Gillon, J. S., Roberts, A. and Griffiths, H.: Determinants of isotopic coupling

431   of CO 2 and water vapour within a Quercus petraea forest canopy, Oecologia, 119(1), 109–119,

432   doi:10.1007/s004420050766, 1999.

433   Hurvich, C. M. and Tsai, C.: Regression and time series model selection in small samples,

434   Biometrika, 76(2), 297–307, doi:10.1093/biomet/76.2.297, 1989.

435   Jochheim, H., Wirth, S. and von Unold, G.: A multi-layer, closed-loop system for continuous

436   measurement of soil CO2 concentration, J. Plant Nutr. Soil Sci., 181(1), 61–68,

437   doi:10.1002/jpln.201700259, 2018.

438   Jost, H.-J., Castrillo, A. and Wilson, H. W.: Simultaneous ^{13}C/ ^{12}C and ^{18}O/ ^{16}O isotope ratio

439   measurements on CO $_2$ based on off-axis integrated cavity output spectroscopy, Isotopes

440   Environ. Health Stud., 42(1), 37–45, doi:10.1080/10256010500503163, 2006.

441   Kammer, A., Tuzson, B., Emmenegger, L., Knohl, A., Mohn, J. and Hagedorn, F.: Application

442   of a quantum cascade laser-based spectrometer in a closed chamber system for real-time δ13C

443   and δ18O measurements of soil-respired CO2, Agric. For. Meteorol., 151(1), 39–48,

444   doi:10.1016/j.agrformet.2010.09.001, 2011.

445   Kato, T., Nakazawa, T., Aoki, S., Sugawara, S. and Ishizawa, M.: Seasonal variation of the

446   oxygen isotopic ratio of atmospheric carbon dioxide in a temperate forest, Japan, ,

447   doi:10.1029/2003GB002173, 2004.

448   Kayler, Z. E., Sulzman, E. W., Rugh, W. D., Mix, A. C. and Bond, B. J.: Soil biology and

449   biochemistry., Pergamon. [online] Available from:

450   https://www.cabdirect.org/cabdirect/abstract/20103097455 (Accessed 16 March 2018), 2010.

451   Keeling, C. D.: The concentration and isotopic abundances of atmospheric carbon dioxide in

452   rural areas, Geochim. Cosmochim. Acta, 13(4), 322–334, doi:10.1016/0016-7037(58)90033-4,

453   1958.

454   Kerstel, E. and Gianfrani, L.: Advances in laser-based isotope ratio measurements: selected

455   applications, Appl. Phys. B, 92(3), 439–449, doi:10.1007/s00340-008-3128-x, 2008.

456   Kuster, T. M., Arend, M., Bleuler, P., Günthardt-Goerg, M. S. and Schulin, R.: Water regime

457   and growth of young oak stands subjected to air-warming and drought on two different forest

458   soils in a model ecosystem experiment, Plant Biol., 15, 138–147, doi:10.1111/j.1438-

459   8677.2011.00552.x, 2013.

460   Kuzyakov, Y.: Sources of CO2 efflux from soil and review of partitioning methods, Soil Biol.

461   Biochem., 38(3), 425–448, doi:10.1016/j.soilbio.2005.08.020, 2006.

462   Levin, I., Graul, R. and Trivett, N. B. A.: Long-term observations of atmospheric CO2 and

463   carbon isotopes at continental sites in Germany, Tellus B, 47(1–2), 23–34, doi:10.1034/j.1600-

464   0889.47.issue1.4.x, 1995.

465   Maier, M. and Schack-Kirchner, H.: Using the gradient method to determine soil gas flux: A

466   review, Agric. For. Meteorol., 192–193, 78–95, doi:10.1016/j.agrformet.2014.03.006, 2014.

467   Mortazavi, B., Prater, J. L. and Chanton, J. P.: A field-based method for simultaneous

468   measurements of the $\delta18O$ and $\delta13C$ of soil CO2 efflux, Biogeosciences, 1(1), 1–9,

469   doi:10.5194/bg-1-1-2004, 2004.

470   Nelson, D. D., McManus, J. B., Herndon, S. C., Zahniser, M. S., Tuzson, B. and Emmenegger,

471   L.: New method for isotopic ratio measurements of atmospheric carbon dioxide using a 4.3 μm

472   pulsed quantum cascade laser, Appl. Phys. B, 90(2), 301–309, doi:10.1007/s00340-007-2894-

473   1, 2008.

474   O'Keefe, A. and Deacon, D. A. G.: Cavity ring-down optical spectrometer for absorption

475   measurements using pulsed laser sources, Rev. Sci. Instrum., 59(12), 2544–2551,

476   doi:10.1063/1.1139895, 1988.

477   Oerter, E. J. and Amundson, R.: Climate controls on spatial and temporal variations in the

478   formation of pedogenic carbonate in the western Great Basin of North America, Geol. Soc. Am.

479   Bull., 128(7–8), 1095–1104, doi:10.1130/B31367.1, 2016.

480   Ohlsson, K., Singh, B., Holm, S., Nordgren, A., Lovdahl, L. and Hogberg, P.: Uncertainties in

481   static closed chamber measurements of the carbon isotopic ratio of soil-respired CO, Soil Biol.

482   Biochem., 37(12), 2273–2276, doi:10.1016/j.soilbio.2005.03.023, 2005.

483   Parameswaran, K. R., Rosen, D. I., Allen, M. G., Ganz, A. M. and Risby, T. H.: Off-axis

484   integrated cavity output spectroscopy with a mid-infrared interband cascade laser for real-time

485   breath ethane measurements, Appl. Opt., 48(4), B73, doi:10.1364/AO.48.000B73, 2009.

486   Parent, F., Plain, C., Epron, D., Maier, M. and Longdoz, B.: A new method for continuously

487   measuring the $\delta^{13}C$ of soil CO$_2$ concentrations at different depths by laser spectrometry, Eur.

488   J. Soil Sci., 64(4), 516–525, doi:10.1111/ejss.12047, 2013.

489 Peltola, J., Vainio, M., Ulvila, V., Siltanen, M., Metsälä, M. and Halonen, L.: Off-axis re-entrant
490 cavity ring-down spectroscopy with a mid-infrared continuous-wave optical parametric
491 oscillator, Appl. Phys. B, 107(3), 839–847, doi:10.1007/s00340-012-5074-x, 2012.

492 Plestenjak, G., Eler, K., Vodnik, D., Ferlan, M., Čater, M., Kanduč, T., Simončič, P. and Ogrinc,
493 N.: Sources of soil CO_2 in calcareous grassland with woody plant encroachment, J. Soils
494 Sediments, 12(9), 1327–1338, doi:10.1007/s11368-012-0564-3, 2012.

495 Ramnarine, R., Wagner-Riddle, C., Dunfield, K. E. and Voroney, R. P.: Contributions of
496 carbonates to soil CO_2 emissions, Can. J. Soil Sci., 92(4), 599–607, doi:10.4141/cjss2011-025,
497 2012.

498 Risk, D. and Kellman, L.: Isotopic fractionation in non-equilibrium diffusive environments,
499 Geophys. Res. Lett., 35(2), L02403, doi:10.1029/2007GL032374, 2008.

500 Satakhun, D., Gay, F., Chairungsee, N., Kasemsap, P., Chantuma, P., Thanisawanyangkura, S.,
501 Thaler, P. and Epron, D.: Soil CO_2 efflux and soil carbon balance of a tropical rubber plantation,
502 Ecol. Res., 28(6), 969–979, doi:10.1007/s11284-013-1079-0, 2013.

503 Schär, C., Vidale, P. L., Lüthi, D., Frei, C., Häberli, C., Liniger, M. A. and Appenzeller, C.:
504 The role of increasing temperature variability in European summer heatwaves, Nature,
505 427(6972), 332–336, doi:10.1038/nature02300, 2004.

506 Schindlbacher, A., Borken, W., Djukic, I., Brandstätter, C., Spötl, C. and Wanek, W.:
507 Contribution of carbonate weathering to the CO_2 efflux from temperate forest soils,
508 Biogeochemistry, 124(1–3), 273–290, doi:10.1007/s10533-015-0097-0, 2015.

509 Schmidt, M. W. I., Torn, M. S., Abiven, S., Dittmar, T., Guggenberger, G., Janssens, I. A.,
510 Kleber, M., Kögel-Knabner, I., Lehmann, J., Manning, D. A. C., Nannipieri, P., Rasse, D. P.,
511 Weiner, S. and Trumbore, S. E.: Persistence of soil organic matter as an ecosystem property,
512 Nature, 478(7367), 49–56, doi:10.1038/nature10386, 2011.

513 Schönwitz, R., Stichler, W. and Ziegler, H.: $\delta 13C$ values of CO_2 from soil respiration on sites
514 with crops of C3 and C4 type of photosynthesis, Oecologia, 69(2), 305–308,
515 doi:10.1007/BF00377638, 1986.

516 Serrano-Ortiz, P., Roland, M., Sanchez-Moral, S., Janssens, I. A., Domingo, F., Goddéris, Y.
517 and Kowalski, A. S.: Hidden, abiotic CO_2 flows and gaseous reservoirs in the terrestrial carbon
518 cycle: Review and perspectives, Agric. For. Meteorol., 150(3), 321–329,

519   doi:10.1016/j.agrformet.2010.01.002, 2010.

520   Sperber, C. Von, Weiler, M. and Büggemann, N.: The effect of soil moisture, soil particle size,
521   litter layer and carbonic anhydrase on the oxygen isotopic composition of soil-released Co2,
522   Eur. J. Soil Sci., doi:10.1111/ejss.12241, 2015.

523   Stevenson, B. A. and Verburg, P. S. J.: Effluxed CO2-13C from sterilized and unsterilized
524   treatments of a calcareous soil, Soil Biol. Biochem., 38(7), 1727–1733,
525   doi:10.1016/j.soilbio.2005.11.028, 2006.

526   Stumpp, C., Brüggemann, N. and Wingate, L.: Stable Isotope Approaches in Vadose Zone
527   Research, Vadose Zo. J., 17(1), 0, doi:10.2136/vzj2018.05.0096, 2018.

528   Sturm, P., Eugster, W. and Knohl, A.: Eddy covariance measurements of CO2 isotopologues
529   with a quantum cascade laser absorption spectrometer, Agric. For. Meteorol., 152, 73–82,
530   doi:10.1016/j.agrformet.2011.09.007, 2012.

531   Tamir, G., Shenker, M., Heller, H., Bloom, P. R., Fine, P. and Bar-Tal, A.: Can Soil Carbonate
532   Dissolution Lead to Overestimation of Soil Respiration?, Soil Sci. Soc. Am. J., 75(4), 1414,
533   doi:10.2136/sssaj2010.0396, 2011.

534   Torn, M. S., Davis, S., Bird, J. A., Shaw, M. R. and Conrad, M. E.: Automated analysis
535   of13C/12C ratios in CO2 and dissolved inorganic carbon for ecological and environmental
536   applications, Rapid Commun. Mass Spectrom., 17(23), 2675–2682, doi:10.1002/rcm.1246,
537   2003.

538   Werner, C. and Gessler, A.: Diel variations in the carbon isotope composition of respired CO2
539   and associated carbon sources: a review of dynamics and mechanisms, Biogeosciences, 8(9),
540   2437–2459, doi:10.5194/bg-8-2437-2011, 2011.

541   Werner, C., Schnyder, H., Cuntz, M., Keitel, C., Zeeman, M. J., Dawson, T. E., Badeck, F. W.,
542   Brugnoli, E., Ghashghaie, J., Grams, T. E. E., Kayler, Z. E., Lakatos, M., Lee, X., M??guas, C.,
543   Og??e, J., Rascher, K. G., Siegwolf, R. T. W., Unger, S., Welker, J., Wingate, L. and Gessler,
544   A.: Progress and challenges in using stable isotopes to trace plant carbon and water relations
545   across scales, Biogeosciences, 9(8), 3083–3111, doi:10.5194/bg-9-3083-2012, 2012.

546   Wingate, L., Ogée, J., Cuntz, M., Genty, B., Reiter, I., Seibt, U., Yakir, D., Maseyk, K., Pendall,
547   E. G., Barbour, M. M., Mortazavi, B., Burlett, R., Peylin, P., Miller, J., Mencuccini, M., Shim,
548   J. H., Hunt, J. and Grace, J.: The impact of soil microorganisms on the global budget of

549   delta18O in atmospheric CO2., Proc. Natl. Acad. Sci. U. S. A., 106(52), 22411–5,

550   doi:10.1073/pnas.0905210106, 2009.

551   Wingate, L., Ogée, J., Burlett, R., Bosc, A., Devaux, M., Grace, J., Loustau, D. and Gessler, A.:

552   Photosynthetic carbon isotope discrimination and its relationship to the carbon isotope signals

553   of stem, soil and ecosystem respiration, New Phytol., 188(2), 576–589, doi:10.1111/j.1469-

554   8137.2010.03384.x, 2010.

555   Yamaoka, K., Nakagawa, T. and Uno, T.: Application of Akaike's information criterion (AIC)

556   in the evaluation of linear pharmacokinetic equations, J. Pharmacokinet. Biopharm., 6(2), 165–

557   175, doi:10.1007/BF01117450, 1978.

558   Zamanian, K., Pustovoytov, K. and Kuzyakov, Y.: Pedogenic carbonates: Forms and formation

559   processes, Earth-Science Rev., 157, 1–17, doi:10.1016/J.EARSCIREV.2016.03.003, 2016.

560

1   Table 1. Correction factor models are fitted for Diff-δ^{13}C, DF (Degrees of Freedom), AIC_C

2   (Akaike information criterion) and [CO_2] CO_2 concentration in ppm

Model Fit	Equation	R^2	AIC_C	DF
Exponential	$Diff - \delta13C = a * (b - \exp(-c * [CO2]))$	0.99	-294.6	54
Polynomial	$Diff - \delta13C = a + b * [CO2] + c/[CO2]\char`\^2)$	0.98	-27.56	54
Logarithmic	$Diff - \delta13C = a + b * ln([CO2])$	0.89	91.68	55
Lowess	------	0.99	-170.24	54

3   Table 2. Correction factor models are fitted for Diff-$\delta^{18}O$, DF (Degrees of Freedom), AIC_C (Akaike information criterion) and $[CO_2]$ CO_2 concentration in ppm.

Model Fit	Equation	R^2	AIC_C	DF
Power	$Diff - \delta 18O\ =\ a*\left(b^{[CO2]}\right)*([CO2]^c)$	0.99	-337.04	51
Polynomial	$Diff - \delta 18O\ =\ (a+b*x)/(1\ +\ c*[CO2]\ +\ d*[CO2]\ \wedge 2)$	0.98	-19.34	50
Stein-Hart	$Diff - \delta 18O\ =\ 1/a + (b*\ln[CO2]) + (c*(ln[CO2])^3)$	0.96	29.77	51
Lowess	-------	0.78	128.66	51

Table 3. Parameter values for correction factor model fit for Diff-δ^{13}C & Diff-δ^{18}O.

Parameter	Value	Std Error	95% Confidence
a^{13}C	31.007	0.2149	30.57 - 31.43
b^{13}C	0.713	0.002376	0.708995 - 0.718522
c^{13}C	0.000043	0.000000	0.000042 - 0.000043
a^{18}O	0.85	0.003	0.8455 – 0.8576
b^{18}O	0.99	0.00	0.999928 – 0.9999283
c^{18}O	0.477	0.0047	0.476871 – 0.478767

Figure 1
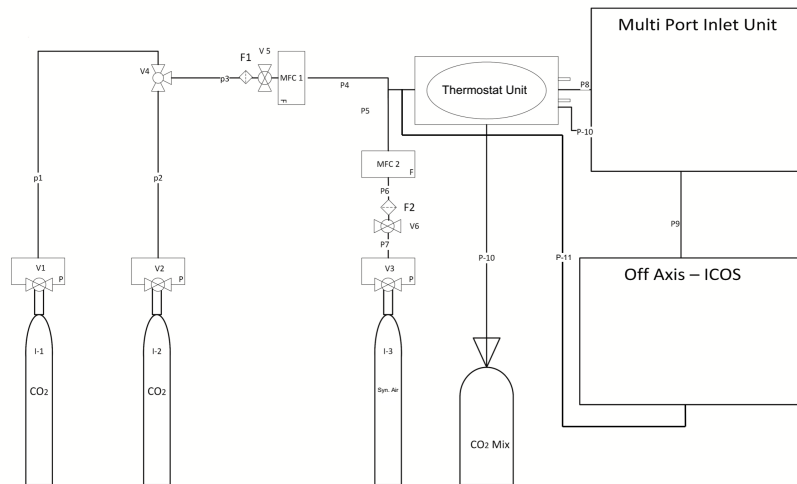
Figure 1: Setup made for calibration of OA- ICOS (LGR-CCIA 36-d). I(1,2): CO2 standards, CO2 Mix: Gas standards mixed in equal molar proportion, I3: Synthetic Air, MFC(1, 2): Mass Flow Controller, F(1, 2): PTFE filter, V(1, 2, 3): Pressure reducing Valves, V4: Three way ball valve, V(5,6): pressure controller valve with safety bypass , P (1-7): Steel pipes, P(8-11):Teflon tubing.

Figure 2
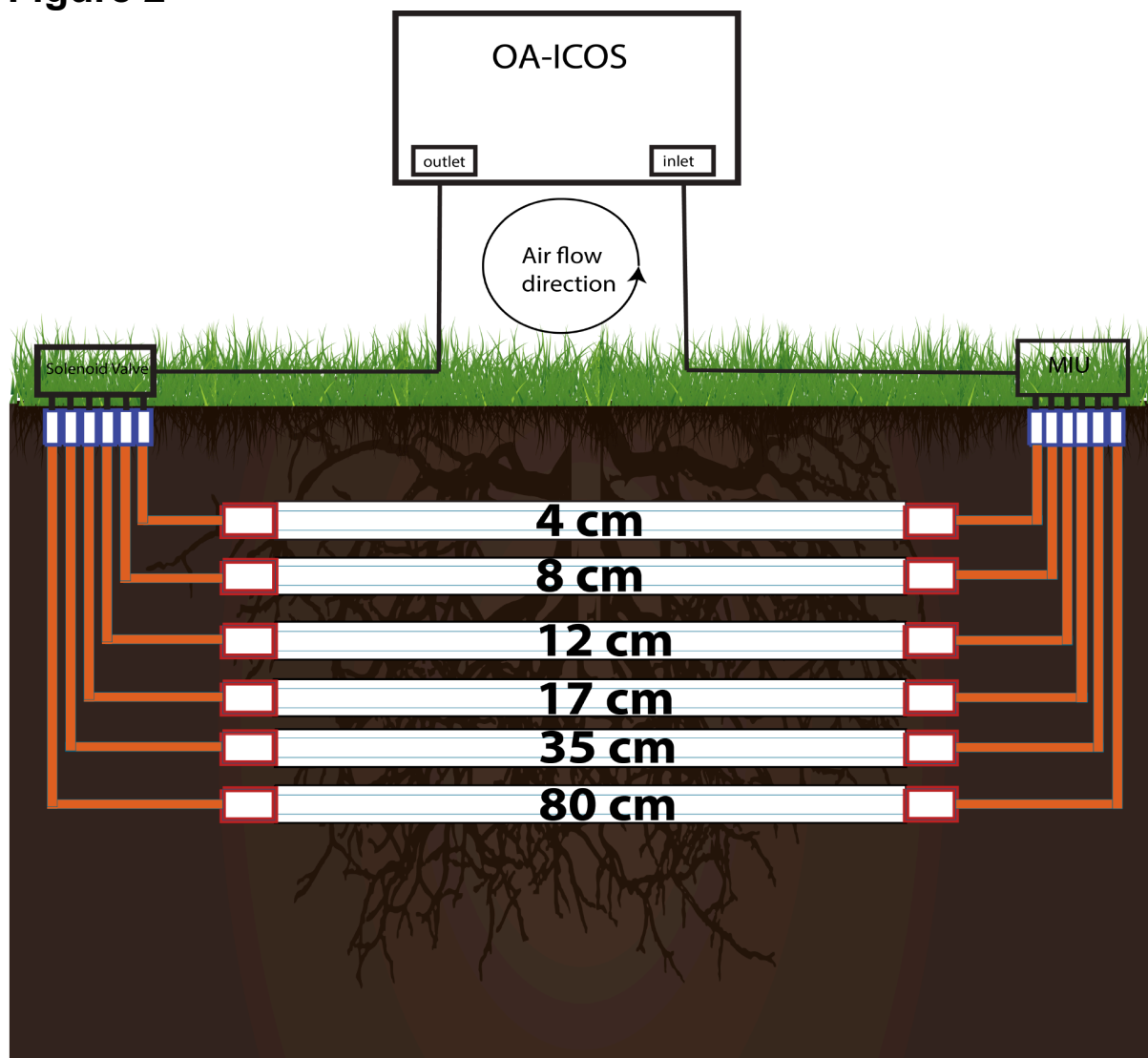
Figure 2: Installation made for soil air CO_2 [ppm], $\delta^{13}C$-CO_2 and $\delta^{18}O$ -CO_2 measurements using an Off-Axis integrated cavity output spectrometer (OA-ICOS). Hydrophobic membrane tubing were installed horizontally in soil at different depths. MIU: multi-port inlet unit

Figure 3
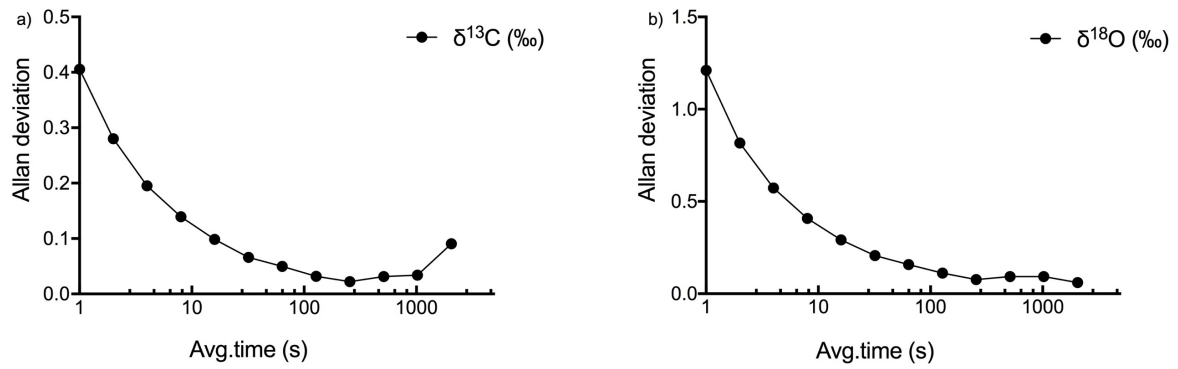
Figure 3: Allan deviation curve for δ¹³C (a) and δ¹⁸O(b) measurements by OA-ICOS CO_2 Carbon isotope analyzer (LGR CCIA-36d).

Figure 4
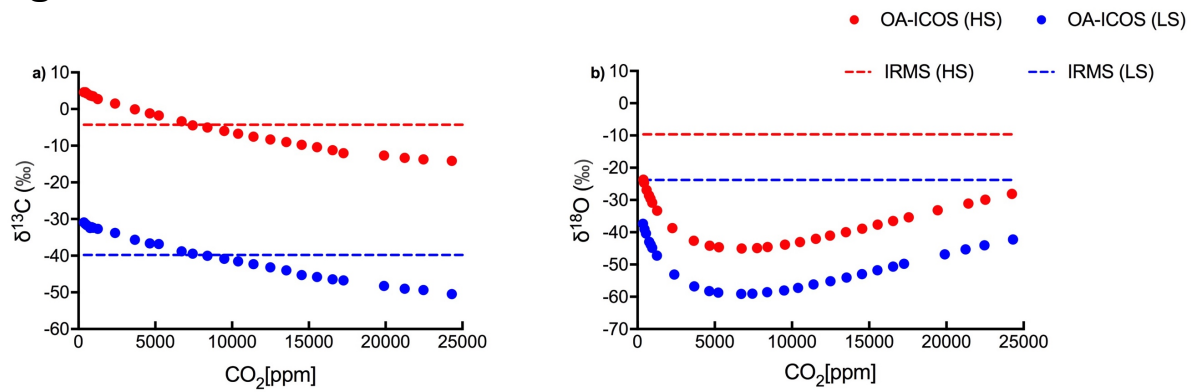
Figure 4: Variability observed in (a) $\delta^{13}C$ and (b) $\delta^{18}O$ measurements using OA-ICOS before calibration. $\delta^{13}C$ and $\delta^{18}O$ measured using OA-ICOS for Heavy Standard and Light Standard are shown as red and blue circles respectively. Actual $\delta^{13}C$ and $\delta^{18}O$ values reported after measuring by IRMS for heavy standard and light standard are shown as red and blue dashed lines respectively.

Figure 5
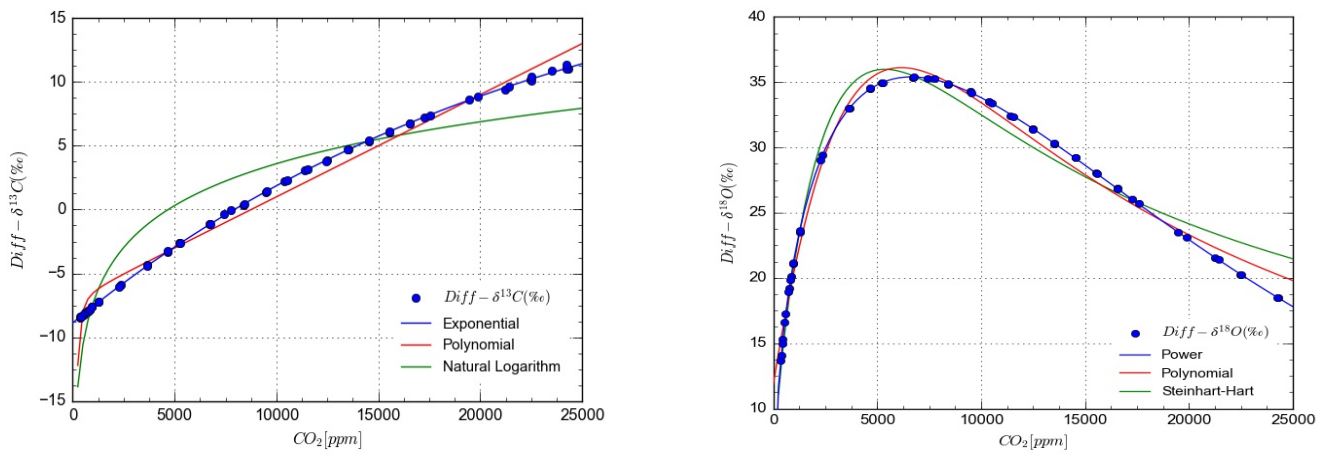
Figure 5: Mathematical models for concentration dependent drift in OA-ICOS measurements of stable isotopes of Carbon (a) and Oxygen (b) in CO_2 from IRMS measurements. Blue circles show Diff-$\delta^{13}C$ (a) and Diff-$\delta^{18}O$ (b) data points and lines represents different mathematical models fitted on the measured data.

Figure 6
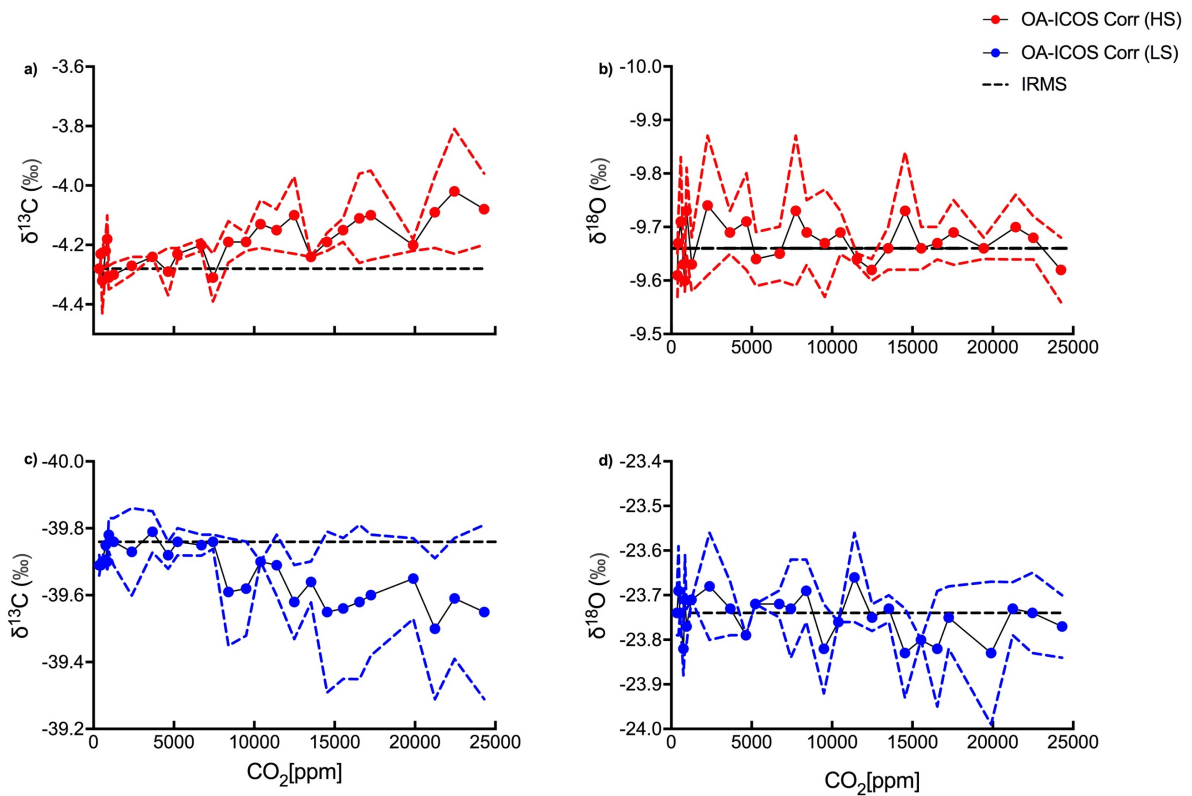
Figure 6: Corrected (a,c) $\delta^{13}C$ and (b,d) $\delta^{18}O$ measurements by OA-ICOS CO_2 Carbon isotope analyzer. $\delta^{13}C$ and $\delta^{18}O$ measured for Heavy Standard and Light Standard are shown as red and blue circles respectively. Actual $\delta^{13}C$ and $\delta^{18}O$ values reported after measuring by IRMS are shown as black dashed lines and 95% confidence intervals are shown as colored dashed lines respectively.

Figure 7
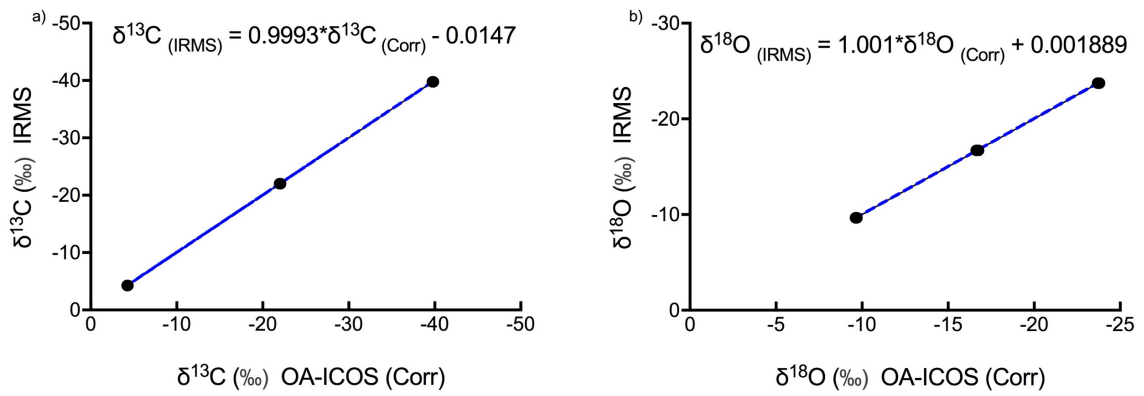
Figure 7: Three point Calibration lines for (a) $\delta^{13}C$ and (b) $\delta^{18}O$ measurements using OA-ICOS with 95% confidence interval.

Figure 8
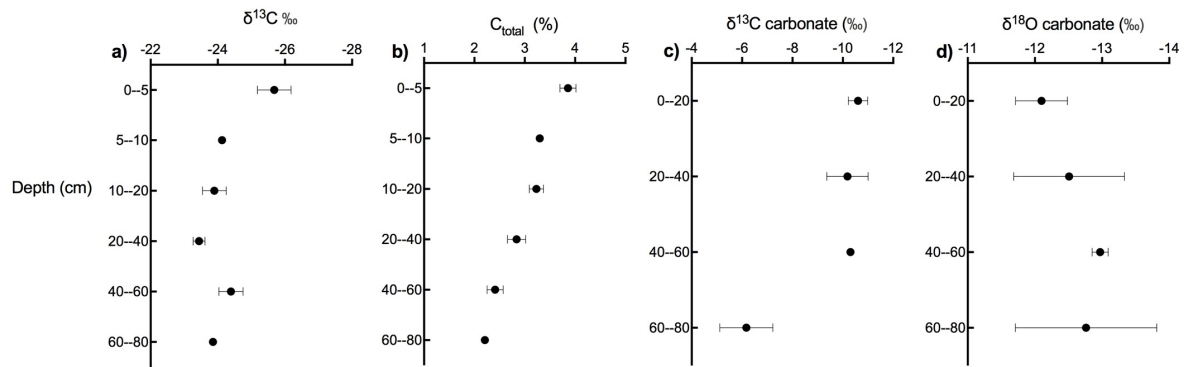
Figure 8: Depth profile of (a) δ¹³C, (b) Carbon content, (c) δ¹³C of soil carbonate and (d) δ¹⁸O of soil carbonate in calcareous soil.

Figure 9
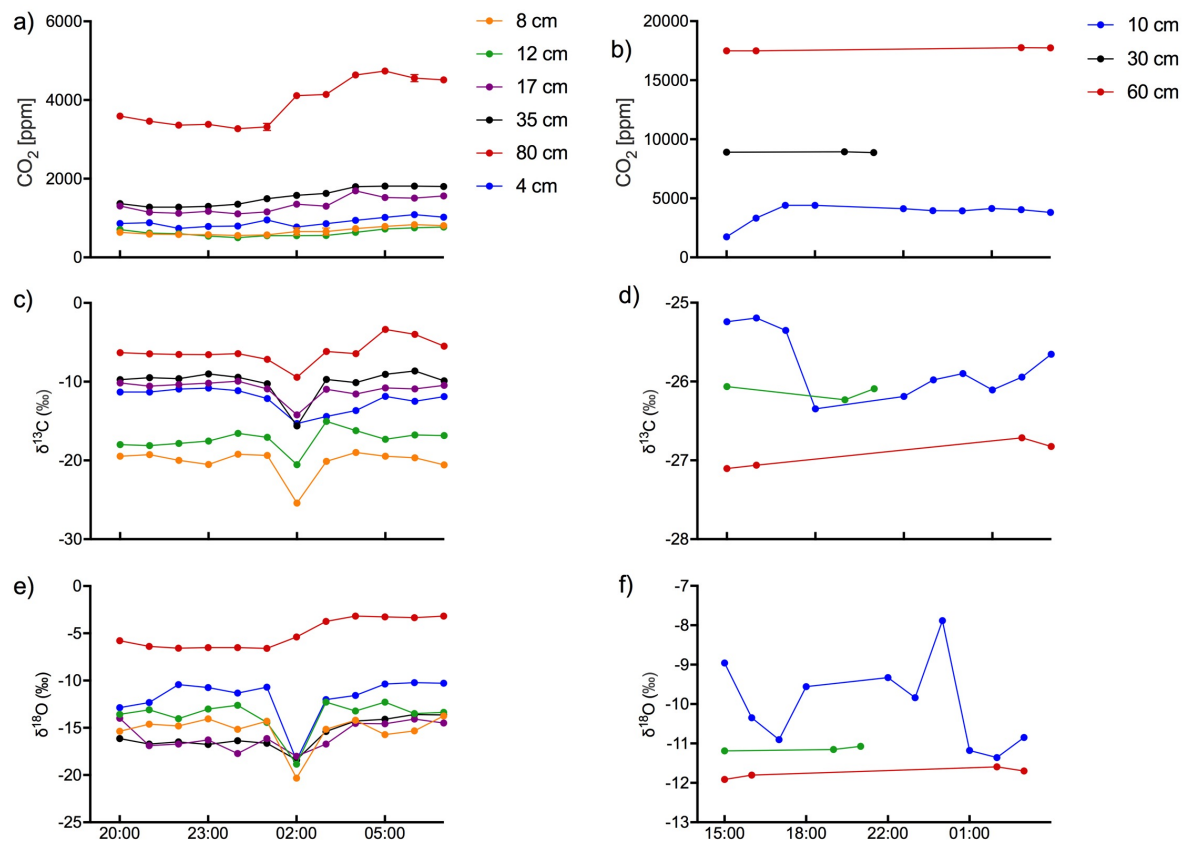
Figure 9: Time course of the evolution of soil gas CO_2 [ppm], $\delta^{13}C$ and $\delta^{18}O$ in calcareous (a,c,e) and acidic (b,d,f) soils. Data collected continuously over a 12 hour time frame for the calcareous soil and a 14 hour time window with intermittent data collection for the acidic soil.

Figure 10
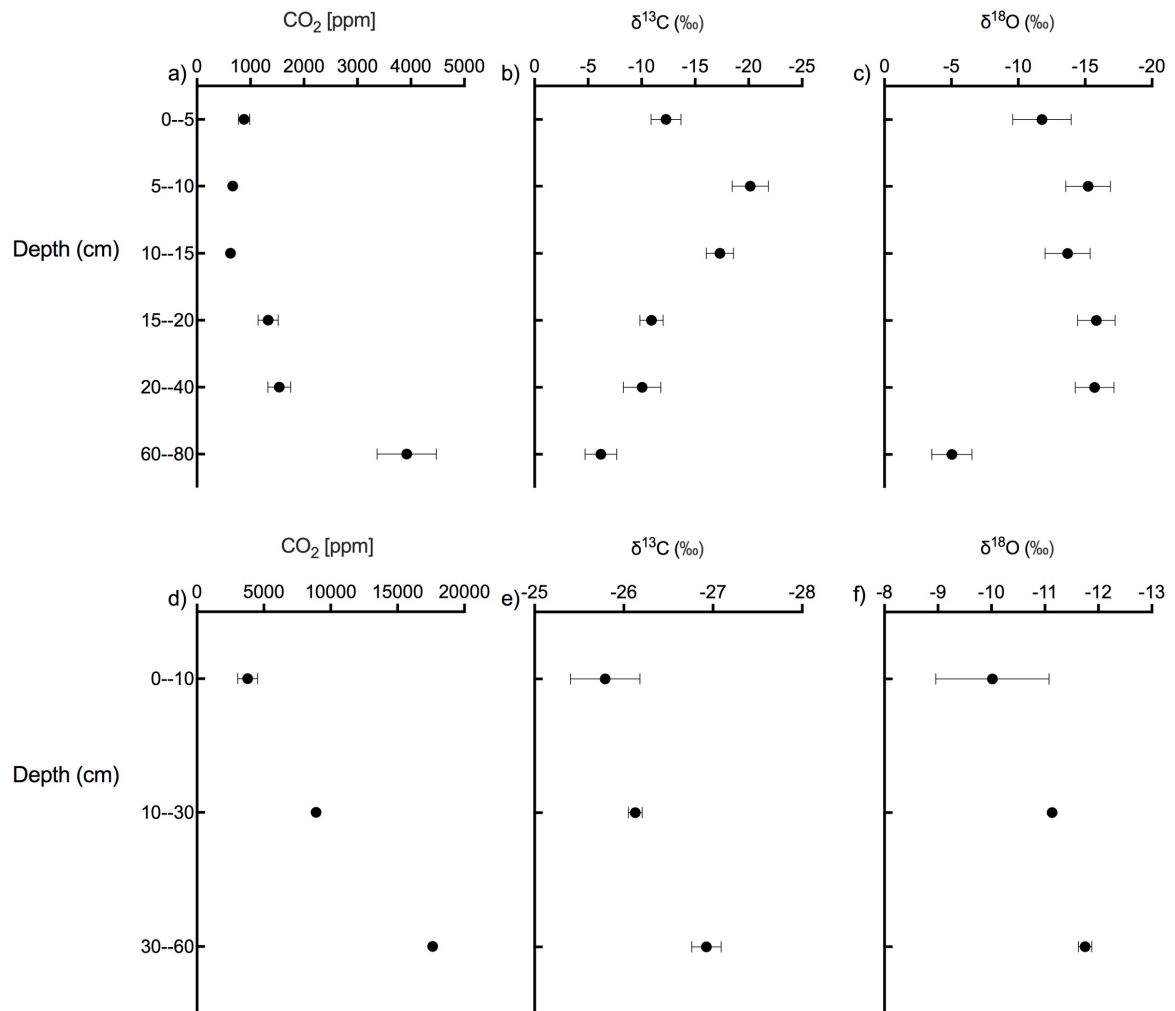
Figure 10: Daily average data of soil CO_2 [ppm], $\delta^{13}C$ and $\delta^{18}O$ in calcareous (a,b,c) and acidic (d,e,f) soils across soil depth profiles.